Stereology of concrete reinforced with short steel fibres

P. STROEVEN
Delft University of Technology
Department of Civil Engineering

Abstract

Mechanical tests on steel fibre reinforced concrete (SFRC) can only be interpreted on the basis of a structural analysis. Stereological tools are available for that purpose. Results of recent investigations will be presented, revealing quite complex characteristics of the fibre dispersion in the matrix. Stereological reasoning can additionally be employed to solve theoretical problems. Such problems are encountered when the constitutive relationships for this type of composites are formulated. Brief reference will be made to typical results obtained in this way.

Introduction

The basically brittle matrix in cementitious materials is incapable of transmitting significant tensile stresses. Even when reinforced by steel bars, the matrix will be unable to accommodate the relatively large deformations the steel bars undergo under tensile loads. Large, widely spaced cracks (as compared to particle size) are the inevitable result. By dispersing slender steel wires through the cementitious matrix, the crack spacing and opening can dramatically be reduced. In doing so, the toughness of the composite is improved by some orders of magnitude.

Theory underlying the constitutive relationships describing mechanical behaviour generally assumes the fibres to be distributed uniformly at random through the matrix. These relationships mostly are of a law-of-mixtures type. A coefficient takes account of efficiency reduction due to the non-linearized fibre distribution. Regression coefficients are introduced to accomplish a best fit to the experimental data [1]. In this way, mechanical behaviour under conditions covered by the tests can be predicted. For design purposes this may be quite efficient.

The evaluation of materials research data, at least, calls for a more detailed insight into actual morphological characteristics of the fibre distribution. It has previously been demonstrated that technological parameters and compaction and placing procedures exert their influences on these characteristics [2, 3]. Mechanical behaviour will manifest itself differently in the various test set-ups in vogue [4, 5].

Technological parameters that may influence fibre distribution in practice are fibre content, vibration time and workability (as influenced by the addition of a superplasticizer). These parameters also directly influence the mechanical properties, of course. Changes in the fibre distribution have to be studied with the help of section or projection images. Previous investigations have already revealed quite complex image patterns [6].

Experimental procedure

Twelve concrete slabs were cast for the experiments. Each slab, 700 mm × 500 mm × 100 mm in size, represents a parameter combination specified in Table 1. A standard aggregate grading with maximum grain size of 8 mm, a cement content of 375 kg/m^3,

Table 1. Investigated parameter combinations in SFRC testing.

fibre content (% by volume) fibres: plain; length 25 mm; diameter 0.38 mm							
	0.0	0.5	1.0	1.5	2.0	2.5	3.0
content of superplasticizer (%); $t = 120$ sec							
0.0	M120	P.1	P.2	P.3			
0.7				P.4	P.10		
1.4				P.5		P.11	
2.0				P.6			P.12
vibration time (sec); V_{pl}=2%							
0	M 0			P.7			
60	M 60			P.8			
120	M120			P.6			
180	M180			P.9			

and a water/cement ratio of 0.5 were employed. The specimens were cut as indicated in Fig. 1 (left).

Four-point bending and splitting tensile tests - the latter in different orthogonal directions - were performed after 28 days. Compressive tests were performed as a reference on 150 mm cubes.

From a methodological standpoint, the researcher has three different strategies at his disposal to approach the problem of analysing details of fibre dispersion.

A direct approach (which in the case of relatively thin elements is also a non-destruc-

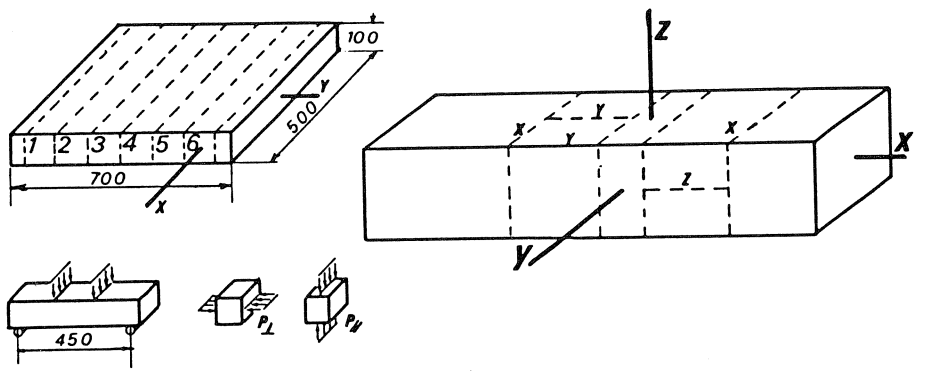

Fig. 1. SFRC slabs were cut into six prisms 100 × 100 × 500 (top left) for the four-point bending testing and thereupon cut into cubes for splitting tensile testing (bottom left). Various section images in three orthogonal directions were subjected to the quantitative image analysis procedure (right).

tive one [7]) consists of X-raying slices of the specimen or structural unit. As demonstrated by Fig. 2, a pattern of lineal features in the projection plane is obtained. The dispersion characteristics can either be determined by simply counting the number of projected fibres (or the projected parts of the fibres, when slices sawn from larger elements are X-rayed [8]), or by counting the number of intersections of the projected (parts of the) fibres and a superimposed line grid. Details of such an approach were previously published [9]. In a wide-ranging research project, in which mechanical and cracking behaviour were studied, the latter approach was chosen [6, 8]. In the present case, a third strategy was adopted. Sections were obtained by cutting the specimens as shown in Fig. 1, on the right. The number of fibre intersections in the section plane was recorded. Hence, we see that all approaches basically rely on *counting*.

Fig. 2. **X-ray pattern of a slice from a SFRC** specimen [8]. The image plane can be subjected directly to a counting operation of the lineal features. Alternatively, intersections can be recorded of these features with a superimposed line grid. For a survey of the methodological aspects involved, see Table 2.

We previously succeeded in analysing such sections directly with the help of an automatic image analyser by making use of the reflective properties of the fibre-cut surfaces [8]. This, however, required careful preparation of the section surfaces by grinding (and if necessary, by polishing) and for anti-corrosion measures. This is quite time-consuming. In the present case we therefore manually copied the section patterns, which were then analysed by the Quantimet 720 (see Figure 3). To that end, the image plane (100×100 mm) was subdivided into strips of equal width (8 and 10 in the respective approaches).

Experimental results

Two representative examples of image patterns are presented in Fig. 4. Visual inspection of such section images already reveals the occurrence of segregation; more wire intersection are found in the bottom part than in the top part of the specimen. The same phenomenon manifests itself in Fig. 2, selected from previous experiments [8]. In addition, however, a relatively small amount of fibre intersections is found in all boundary zones in the present experiments. Since the extension of this zone should theoretically be half the fibre length (i.e. 12.5 mm in this case), we used eight strips to analyse the magnitude of the boundary effect. The Quantimet's readings are fed into a PDP-computer for further processing.

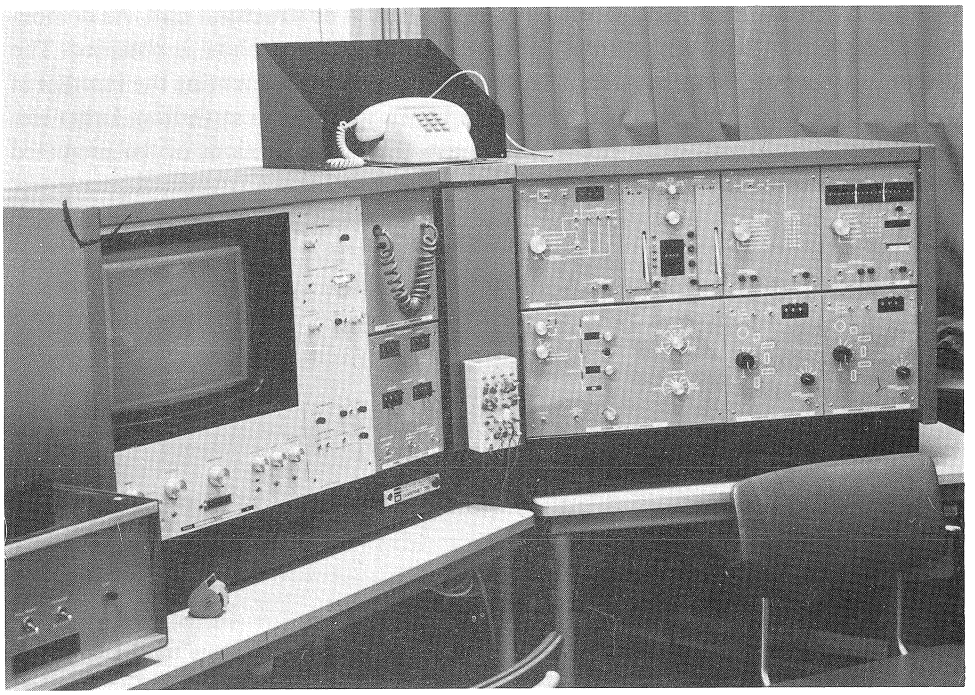

Fig. 3. Quantimet 720 (automatic image analyser) used for the investigations.

Fig. 5 (left) presents some of the primary results concerned with the fibre distribution over the height of the cross-section of the specimens. By comparing such block diagrams it is possible to visualize the effect of fibre content, vibration time and workability. This is demonstrated by an example shown in Fig. 5 (right). It relates to SFRC specimens containing 1.5% of steel fibres. The effect of compaction on the distribution of

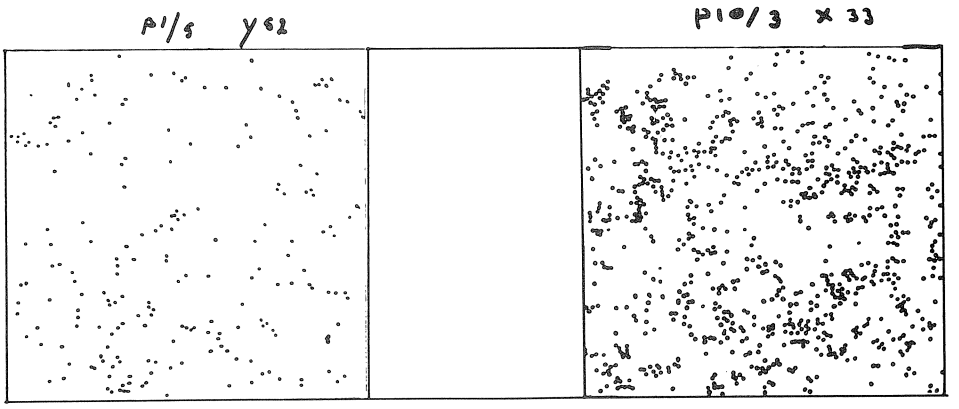

Fig. 4. Section images of SFRC specimens containing 0.5% (left) and 2% (right) by volume of steel fibres. Segregation and boundary effects are visible.

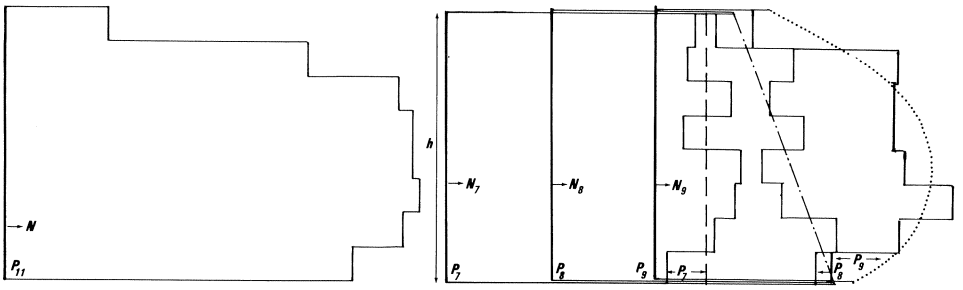

Fig. 5. Distribution of fibres over the height of SFRC specimens. The respective values per strip are shown on the left. On the right, the results are shown of specimens containing 1.5% by volume of fibres, but compacted for 0, 60 and 180 sec., respectively.

the fibres over the height of the specimens has been plotted. An initially rather uniform distribution of the fibres is modified by 60 sec of compaction into a non-uniform distribution; more fibres are localized in the bottom half than in the top half. This effect is slightly more pronounced in the curve representing the experimental values of the number of fibre intersections over the height of the cross-section of a specimen vibrated for 180 sec.

In Fig. 6 we have assembled all the parabolic regression curves in consecutive order (though volume fraction of wires, roughly speaking, increases toward the right in the diagram). We see that boundary and segregation effects increase with volume fraction of fibres. The curves represent average values for all sections containing in their plane the z-axis (see Fig. 2). The segregation effect is absent, of course, in sections perpendicular to the z-axis, the so called z-planes.

Increase of curvature of the regression lines with volume fraction seems to be roughly proportional in Fig. 6. This is confirmed by calculations. For practical (i.e. design) purposes it would therefore be appropriate to derive a single curve, normalized for fibre content, from the experiments. Segregation and boundary effects nevertheless depend

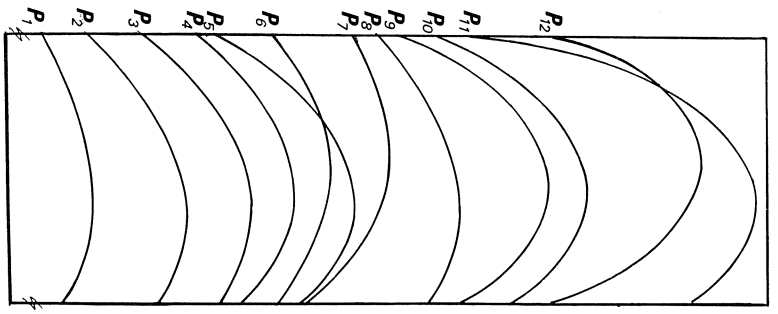

Fig. 6. Parabolic regression curves revealing the distribution of fibres over the height of SFRC specimens. P.1–P.12 represent the parameter combinations specified in Table 1. The curves are drawn to the same scale with volume fraction on the horizontal axis; however, the zero values do not correspond.

to some extent on the technological parameters considered. Fig. 7 presents some of the results in graphical form. The values of S and B are derived from the regression curves as explained in the caption of Fig. 7, on the left.

S is the change in fibre density per unit of the specimen height (for convenience expressed in decimeters, since $h \cong 1$). We see that for practical values of the volume fraction of fibres, say 0.5–1.5%, $2hS$ is around 0.25.

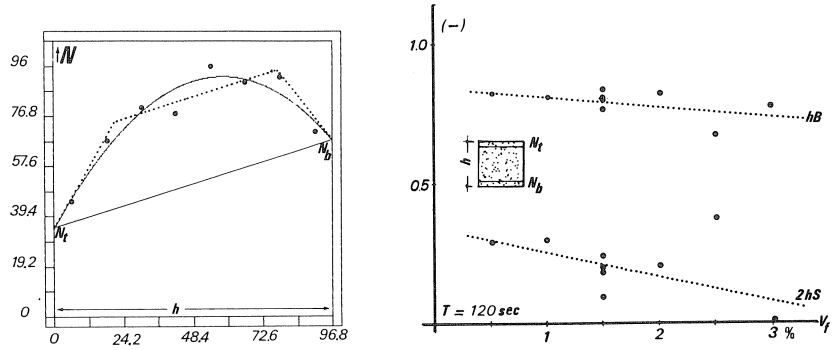

Fig. 7. (left) Number of features (fibres), N, per strip (12.5 mm × 100 mm) as varying over the height, h, of a SFRC specimen. Parabolic and tri-lineal regression lines are shown. Fig. 7 (right) gives the experimental results on segregation ($2hS$) and boundary effect (hB) defined by

$$S = (N_b - N_t)/2h\bar{N}$$

$$B = (N_b + N_t)/2h\bar{N}$$

N_b and N_t are the extrapolated number of fibre intersections at the bottom and top, respectively. $\bar{N}$ is a sample mean value for N.

B is defined as the ratio of average fibre density in the boundary layers to overall density, per unit of the specimen height. We see that hB attains values around 0.8. For evenly distributed fibres - conventionally assumed in theroretical approaches - S and B would have been zero and unity, respectively.

Parabolic regression curves have been determined for all sections in the two coordinate directions. Fig. 7 (left) presents a single example. Due to preparation in larger slabs the results of so-called x- and y-planes were quite similar and have therefore been combined in determining average curves as shown in Fig. 6.

Anisometry and anisotropy

Three-dimensional morphological features of the fibre structure can be derived from the 2-D characteristics in the sampled plane. Stereology offers the geometrical-statistical basis for relating the required 3-D features to the 0-D information yielded by the counting operations.

Partially oriented structures generally require random sampling. Apart from being time consuming, the cutting operations would be complicated. It has proved to be sufficiently accurate to assume the actual fibre distribution to be governed by a mixture of 2-D and 3-D fibre portions. In the more general case, when there would be a significant deviation from the state of rotational symmetry, it would be possible to add a 1-D portion as well. In such cases all morphological parameters (such as fibre content) will be linear functions of the three fibre portions. This will require performing three independent measurements (counting operations). The relevant theoretical framework has been developed by the present author [4, 9]. Table 2 gives a survey.

By taking a zero value for the lineal portion, the formulas for a two-component system are obtained. For such a system we have for the degree of orientation ω [6, 10]

$$\omega = (N_x - N_z) / (N_x + 0.273\ N_z) \tag{1}$$

in which N_x and N_z are the number of fibre intersections in the x- and z-planes, respectively.

Although N_x (and N_y) vary over the height of the specimen, this only leads to second-

Table 2. Theoretical basis for quantitative image analysis in the case of fibre reinforced cementitious materials. Three experimental approaches, based on section and projection analysis, are presented.

method of analysis	nature of image	stereological relationships	
feature counting	section	$P_{Ax} = \frac{1}{2}L_{Vi} + \frac{2}{\pi}L_{Vp} + L_{Vl}$	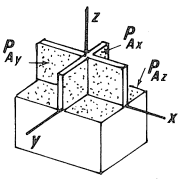
		$P_{Ay} = \frac{1}{2}L_{Vi} + \frac{2}{\pi}L_{Vp}$	
		$P_{Az} = \frac{1}{2}L_{Vi}$	
feature counting	projection	$N'_{Ax} = \frac{t}{l}L_V + \frac{1}{2}L_{Vi} + \frac{2}{\pi}L_{Vp} + L_{Vl}$	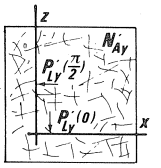
		$N'_{Ay} = \frac{t}{l}L_V + \frac{1}{2}L_{Vi} + \frac{2}{\pi}L_{Vp}$	
		$N'_{Az} = \frac{t}{l}L_V + \frac{1}{2}L_{Vi}$	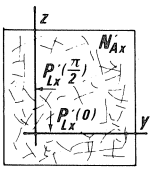
intersection counting	projection	$P'_{Lx}(0) = \frac{1}{2}L_{Vi}t$	
		$P'_{Lx}(\frac{\pi}{2}) = (\frac{1}{2}L_{Vi} + \frac{2}{\pi}L_{Vp})t$	
		$P'_{Ly}(0) = \frac{1}{2}L_{Vi}t$	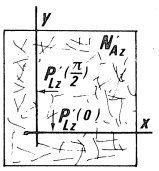
		$P'_{Ly}(\frac{\pi}{2}) = (\frac{1}{2}L_{Vi} + \frac{2}{\pi}L_{Vp} + L_{Vl})t$	
		$P'_{Lz}(0) = (\frac{1}{2}L_{Vi} + \frac{2}{\pi}L_{Vp})t$	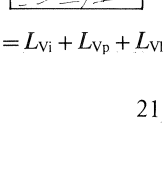
		$P'_{Lz}(\frac{\pi}{2}) = (\frac{1}{2}L_{Vi} + \frac{2}{\pi}L_{Vp} + L_{Vl})t$	

$L_V = L_{Vi} + L_{Vp} + L_{Vl}$

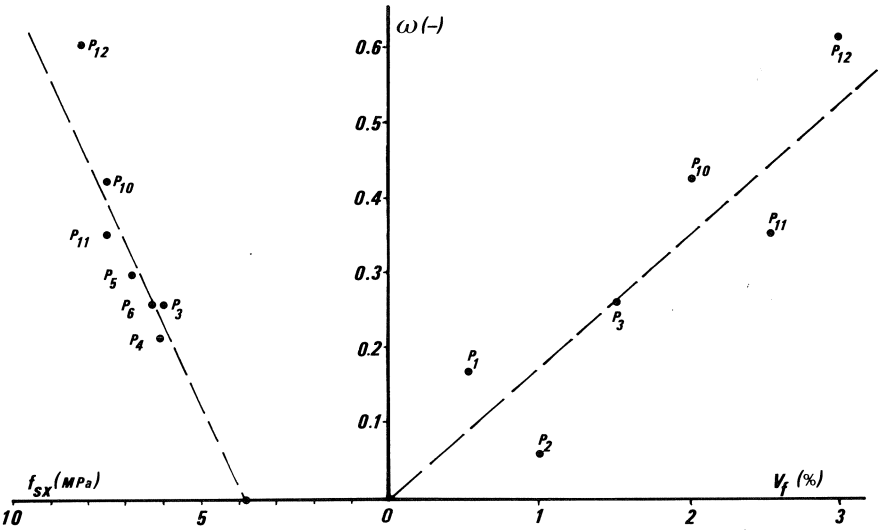

Fig. 8. The degree of orientation, $\bar{\omega}$, of a partially oriented fibre structure in SFRC is controlled by the volume fraction of fibres (right). Apart from depending on the volume fraction of fibres, the splitting tensile strength, f_{sx} is also related to the degree of orientation.

order effects in the splitting tensile strength. Average values are therefore determined for ω. Such values are used in Fig. 8. The same interpretation should be given to the values of ω used in Table 3.

Table 3 illustrates the effect of partial orientation (anisometry), and of different bonding conditions between steel and concrete, on the splitting tensile strength. We may safely conclude that knowledge of the degree of orientation in the fibre reinforcement is indispensable to the correct interpretation of strength data. The data presented in Table 3 are derived from the constitutive relationships [4]

$$f_{sx} = \tfrac{1}{6} a\tau V_f (1 + \tfrac{1}{2}\omega) + \sigma_m V_m \tag{2}$$

$$f_{sz} = \tfrac{1}{6} a\tau V_f (1 - \omega) + \sigma_m V_m \tag{3}$$

Table 3. Strength ratio, f_{sx}/f_{sz}, as influenced by the bonding conditions between steel and concrete and by the partial fibre orientation, ω.

	τ/σ_m					
ω	2	3	4	5	6	
0	1.0	1.0	1.0	1.0	1.0	
0.1	1.05	1.08	1.10	1.12	1.15	
0.2	1.10	1.15	1.20	1.25	1.30	f_{sx}/f_{sz}
0.3	1.15	1.22	1.30	1.38	1.45	
0.4	1.20	1.30	1.40	1.50	1.60	
0.5	1.25	1.38	1.50	1.62	1.75	
0.6	1.30	1.45	1.60	1.85	1.90	

Essential elements of the derivation of these constitutive relationships are presented in an Appendix.

In eqs (2) and (3) τ is the interfacial shear strength, a, V_f and ω are the aspect ratio, volume fraction and degree of orientation of the fibres, σ_m is the mortar strength and V_m equals the fraction of the cross-sectional area transmitting tensile sresses. The linear dependency of f_{sx} on $\bar{\omega}$ is confirmed by the experimental results, as shown in Fig. 8, at the left.

The experimental data on strength, compiled in a condensed form in Table 4, reveal a considerable degree of anisotropy. By adding 1.5% by volume of fibres, an increase in the splitting tensile strength in the z-direction of roughly 20 to 30% is obtained. In the x-direction these values are raised to 60 to 70%. This is in quantitative agreement with eqs. (2) and (3), using values for $\bar{\omega}$ determined by the image analysis.
We can specify the agreement more accurate. The linear dependence of $\bar{\omega}$ on V_f can be expressed by

$$\bar{\omega} = cV_f \quad (c = \text{constant}) \tag{4}$$

Upon substitution of eq. (4) into eqs. (2) and (3) we obtain the parabolic relationships

$$f_{sx} = \tfrac{1}{6}a\tau V_f(1 + \tfrac{1}{2}cV_f) + \sigma_m V_m \tag{5}$$

$$f_{sz} = \tfrac{1}{6}a\tau V_f(1 - cV_f) + \sigma_m V_m \tag{6}$$

In the case of a random uniform fibre dispersion we would have found

$$f_{sx} = f_{sz} = \tfrac{1}{6}a\tau V_{fnom} + \sigma_m V_m \tag{7}$$

where V_{fnom} is the nominal fibre content.

Due to rearrangement of the fibres in experimental conditions, we see that the effective fibre reinforcement in a favourable cross-section (x-plane) increases up to $V_f(1 + \frac{1}{2}cV_f)$, while in an orthogonal plane (z-plane) the effective fibre reinforcement is diminished to $V_f(1 - cV_f)$. These factors contain the influence of areal fibre density (N_A is the number of fibres per unit of area) and orientation distribution. Changes in N_A are slightly smaller than in V_f. It can easily be demonstrated that N_{Anom} for the case of a random uniform system is increased by partial fibre orientation in the x-plane to $N_{Anom}(1 + \frac{1}{2}cV_f)/(1 + 0.273cV_f)$. In the z-plane the decline is also slightly smaller. The expected number of fibre intersections per unit of area will be $N_{Anom}(1 - cV_f)/(1 + 0.273cV_f)$. Since $\bar{\omega}$ attains for practical values of the volume fraction of fibres values up to about 0.4, the changes in N_{Ax} and N_{Az} quite accurately reveal the changes in effective reinforcement in these directions due to partial orientation of the fibres.

The results of the quantitative image analysis confirm the theoretical predictions as is shown by Fig. 9. Anisometry of the fibre structure increases progressively upon increase of the fibre content.

The experimental results for the splitting tensile strength, compiled in Table 4, manifest a similar improvement when the volume fraction of fibres is increased. Some deviations occur solely due to a detrimental effect of the fibres on the mortar strength σ_m.

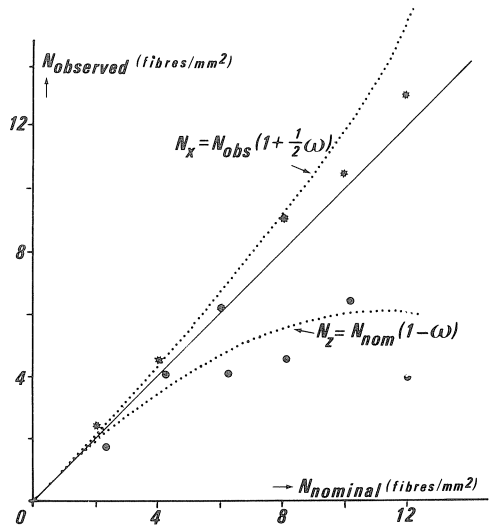

Fig. 9. Fibre anisometry observed by quantitative image analysis in SFRC specimens.

Hence, we see that anisometry in the fibre structure is directly reflected in anisotropic behaviour of the fibre composite!

Bending strength is even more improved by adding fibres than the splitting tensile strength in the same direction. This is definitely the result of the segregation of the fibres [12]. The constitutive relationships are more complicated in that case, however [5]. It can be shown, nevertheless, that theory and experiments lead to similar values for the bending strength, when the values for S and $\bar{\omega}$ given in this paper are used

Boundary effect

The detection of a significant boundary effect that will give rise to a size effect in specimens and structural elements (particular in the case of thin or small ones) called

Table 4. Data on the influence of technological parameters (fibre content, amount of superplasticizer) on bending and splitting tensile strength of SFRC specimens, revealing the effect of partial orientation and segregation of the fibres. Vibration time is in all cases 120 sec. CV is the coefficient of variation.

series number	nominal wire content %	content of super-plasticizer %	modulus of rupture perpendicular f_{bx} N/mm²	CV %	strength increase due to fibres -	splitting tensile strength perpendicular f_{sx} N/mm²	CV %	parallel f_{sz} N/mm²	CV %	strength increase due to fibres -	strength increase due to fibres -
M	0.0	0.0	3.03	4.6	1.0	3.58	2.8	3.82	4.7	1.0	1.0
P.3	1.5	0.0	5.24	8.0	1.74	4.45	3.6	5.98	12.9	1.24	1.56
P.4	1.5	0.7	5.30	13.9	1.75	4.66	9.0	6.13	15.6	1.30	1.60
P.5	1.5	1.4	5.95	8.9	1.96	4.63	9.7	6.79	9.6	1.29	1.77
P.6	1.5	2.0	6.37	10.8	2.10	4.13	6.5	6.37	9.3	1.15	1.66
P.10	2.0	0.7	5.53	8.5	1.83	4.61	7.2	7.51	11.7	1.29	1.96
P.11	2.5	1.4	6.25	9.4	2.06	4.73	6.7	7.54	11.0	1.32	1.97
p.12	3.0	2.0	6.77	8.7	2.23	3.53	5.1	8.18	15.2	0.98	2.14

for a theoretical description of this phenomenon. In the literature only 2-D solutions are available [13]. Proceeding as outlined above, we analytically determined solutions for 2-D and 3-D portions separately. By superimposing these solutions it is possible to construct more general solutions for partially-planar oriented structures.

The procedure will be briefly described. Details will be given elsewhere. The boundary zone is hypothetically assumed to be sliced. The very thin slices all run parallel to the outer surface of the boundary layer of the specimen. Next, imagine all fibres whose centres are contained in slice (i) to be gathered together, while preserving their original orientation. By joining the ends of these fibres, the other fibre ends would uniformly at random cover the surface of a sphere with radius l (= fibre lenght), in the case of a 3-D dispersion. For a 2-D SFRC composite we would obtain a circle with a radius l.

When (i) is remote from the external surface, the sphere and circle would be "complete". Upon approaching the external surface, particular fibres would intersect the outer surface. As a result, we have to exclude sectors in the sphere or circle, when dealing with a 3-D or 2-D fibre composite, respectively. These excluded parts increase in size when (i) approaches the external surface. Hence, the elementary portions of the partially-planar model will manifest a growing deviation from 3-D and 2-D uniform randomness.

The contributions to stiffness or strength of the fibres encompassed by the "incomplete" sphere or circle models can easily be determined. In the first case we consider the contribution to stiffness parallel to the outer surface by sampling a unit volume. In the second case we consider the conditional probability of those fibres of the above-mentioned set which intersect a crack surface perpendicular to the outer surface. Care has to be bestowed on selecting the correct upper and lower bounds of the otherwise elementary integrals involved.

Following the same reasoning, stiffness and strength contributions of a slice (i) can be extended to a surface layer with a finite thickness $x(0 \leqq x \leqq \frac{1}{2}l)$. To that end, we have to correct the fibre length in the sphere and circle models to such an extent, that only the parts of the fibres contained in the boundary layer considered are taken into account. For crack growth studies, in particular, this seems a relevant approach, since the stiffness as well as the efficiency of the reinforcement diminish towards the external surfaces of the specimens or structural units. The 2-D portion should be considered, of course, only in those cases where the plane of orientation is perpendicular to the external surface (or more accurately, is not parallel to this surface).

Conclusions

Stereology offered the tools for successfully analysing the quite complex distribution of fibres in SFRC composite specimens used for these investigations. The fibres in the slab-like specimens were disposed in a partially-planar structure with the axis of symmetry in the direction of the gravity field. More fibres were present in the interior than in the boundary layers. Due to compaction of the fresh mixes, fibres also moved down to a certain extent, causing some segregation.

In this way, a more intelligent basis can be given to strength results in bending and splitting tensile modes. Anisotropy was shown in the experiments to be mainly governed by anisometry of the fibre structure. The disproportionate increase in the bending strength as compared with the splitting tensile strength is due to the segregation effect.

In this paper the image analysis aspects have been particularly emphasized. In Babut's paper the mechanical aspects will receive full attention. Both relate to the same experiments performed in the Stevin Laboratory during a four-month stay of Dr. Babut.

References

1. Swamy, R. N., P. S. Mangat and C. V. S. K. Rao (1974). The mechanics of fibre reinforcement of cement matrices. ACI Spec. publ. SP-44, pp. 1-28.
2. Edgington, J. and D. J. Hannant (1972). Steel fibre reinforced concrete. The effect on fibre orientation of compaction by vibration. Mat. Constr., 5, 25, pp. 41-44.
3. Stroeven, P. (1979). Morphometry of fibre reinforced cementitious materials. Mat. Constr., 12, 67, pp. 9-20.
4. Stroeven, P. (1982). Some structural aspects of the tensile properties of SFRC. In: Proc. concretes reinforced by dispersed fibres. Ostrava, pp. 32-45.
5. Stroeven, P. (1980). Tensile behaviour of fibre reinforced cementitious materials as affected by fibre distribution parameters. Mikroskopie, 37, pp. 335-338.
6. Stroeven, P. and S. P. Shah (1978). Use of radiography-image analysis for steel fibre reinforced concrete. In: Proc. RILEM Symp. Testing and test methods of fibre cement composites. Sheffield. The Construction Press Lancaster, pp. 345-353.
7. Kasperkiewicz, J., B. Malmberg and A. Skarendahl (1978). Determination of fibre content, distribution and orientation in steel fibre concrete by X-ray technique. In: Proc. RILEM Symp. Testing and test methods of fibre cement composites, Sheffield. The Construction Press, Lancaster, pp. 297-314.
8. Stroeven, P., H. W. Reinhardt and H. A. Körmeling (1979). Fibre concrete. Heron, 24, pp. 1-63.
9. Stroeven, P. (1983). Some methodological aspects of morphometry in materials technology. Acta Stereol. 2/Suppl. I, pp. 201-204.
10. Underwood, E. E. (1968). Surface area and length in volume. In: Quantitative metallurgy. Eds. de Hof, R. I., F. N. Rhines. McGraw Hill Book Co.
11. Naaman, A., E. F. Moavenzadeh and J. McGarry (1984). Probabilistic analysis of fibre reinforced concrete. J. Eng. Mech. Div. ASCE, EM 2, April, pp. 397-431.
12. Bonzel, J. and M. Schmidt (1984). Verteilung und Orientierung von Stahlfasern im Beton und ihr Einfluss auf Eigenschaften von Stahlfaserbeton. Betontechn. Berichte, Beton, 11, pp. 463-470; 12, pp. 501-504; (985), 1, pp. 27-32.
13. Kameswara Rao, C. V. S. (1979). Effectiveness of random fibres in composites. Cem. Concr. Res., 9, pp. 685-693.

APPENDIX

Essential elements in the derivation of the constitutive relationships for the splitting tensile strength of SFRC composites.

Adopting the sphere and circle models described in the paper under the heading "BOUNDARY EFFECT" we proceed as follows:

- a wire intersecting a crack has an embedded part $l_i (l_i \leqslant l - l_i)$, see Fig. 10;
- we assume a triangular distribution of the shear stress in the interfacial layer between steel and mortar; the maximum stress corresponds to the maximum shear strength

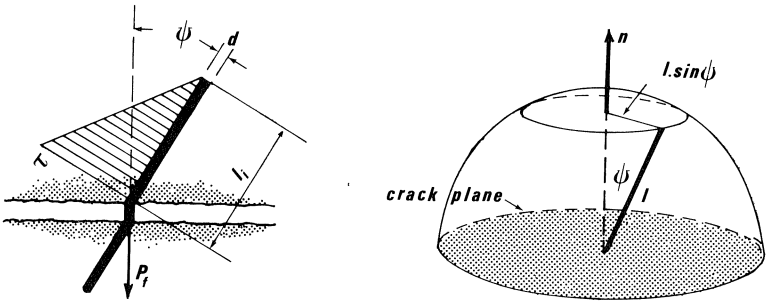

Fig. 10. A single crack transmitting a load at a crack surface (left). All wires intersecting the crack plane are gathered together, maintaining their original orientation, and all jointed at one end. The other ends will cover the surface of a sphere shown at the right. The infinitely small surface element of the sphere associated with a single wire is proportional to sin ψ.

τ of the interface; this maximum is achieved at the point where the wire protrudes from the crack surface;

- as a consequence, the load carried by a single wire is

$$P_f = \tfrac{1}{2}\pi \, d\tau l_i \cos \psi,$$

ψ being the angle between the wire and the normal vector to the crack plane. Per unit area of the crack surface we have N_A wires, so that the stress transmitted at the crack surface by the wires is

$$\sigma_f = \tfrac{1}{2}\pi \, d\tau N_A \overline{l_i \cos \psi}$$

- for 3-D and 2-D portions we have respectively

$$N_{Ai} = \tfrac{1}{2} L_{Vi} \text{ and } N_{Ap} = \frac{1}{\pi} L_{Vp} \quad (i = \text{isometric}, \; p = \text{planar portion})$$

- L_v is the total wire length per unit of volume;
- from the sphere model it is obvious that

$$\overline{l_i \cos \psi} = \tfrac{1}{4} l \int_0^{\pi/2} \sin \psi \cos^2 \psi \, d\psi \Big/ \int_0^{\pi/2} \sin \psi \cos \psi \delta\psi = \tfrac{1}{6} l$$

- proceeding similarly for the 2-D portion yields

$$\overline{l_i \cos \psi} = \tfrac{1}{4} l \int_0^{\pi/2} \cos^2 \psi \, d\psi \Big/ \int_0^{\pi/2} \cos j \, d\psi = \frac{\pi}{16} l$$

- upon substitution of N_A and $\overline{l_i \cos \psi}$ we obtain

$$\begin{aligned} \sigma_i &= \tfrac{1}{24} \pi d \, l \tau L_{Vi} \\ \sigma_p &= \tfrac{1}{16} \pi d \, l \tau L_{Vp} \; + \\ \hline \sigma_x &= \tfrac{1}{48} \pi d \, l \tau (2 L_{Vi} + 3 L_{Vp}) \end{aligned}$$

- by definition we have $L_{Vp} = \omega L_V$ and $L_{Vi} = L_V - L_{Vp} = (1 - \omega) L_V$
- substitution in the herefore given formula finally yields

$$\sigma_x = \tfrac{1}{6} \tau a V_f (1 + \tfrac{1}{2} \omega)$$

- for the z-direction a similar procedure can be adopted.